Magnetically induced decomposition in Co-Cr thin-film and bulk alloys

Astrid Pundt
Institut für Metallphysik, Hospitalstraße 3-7, 37073 Göttingen, Germany

Carsten Michaelsen
Institut für Werkstofforschung, GKSS-Forschungszentrum, 21502 Geesthacht, Germany

(Received 4 June 1997)

It has been reported in recent years that composition modulations on a ten nanometer scale with unknown origin occur in Co-Cr alloy thin films. In the present investigation, we intend to analyze the origin of these concentration modulations. Sputtered thin films as well as bulk samples both with compositions of about 20 at. % Cr were analyzed by transmission electron microscopy and by field-ion microscopy equipped with atomic-probe mass spectrometry. The experimental results show that composition modulations are present in both types of alloys, with the concentration varying between 8 and 40 at. % Cr. The length scale of the composition modulations is approximately 10 and 40 nm for the thin film and the bulk samples, respectively. The results are interpreted in terms of the thermodynamics and kinetics of the system. Calculations of the thermodynamic functions of the system show that at high Co concentrations, the occurrence of magnetism leads to a downwards curvature of the Gibbs energy vs concentration curves. As a result of this magnetic stabilization at Co-rich concentrations, a metastable miscibility gap occurs that explains the tendency for phase separation into ferromagnetic and paramagnetic phases. The diffusivity of the system was examined using multilayer thin-film diffusion couples, and the results indicate that grain-boundary diffusion is responsible for the fast decomposition process observed. It is concluded that decomposition takes place by a discontinuous precipitation process that starts from grain boundaries. [S0163-1829(97)04146-5]

I. INTRODUCTION

In 1978 Iwasaki and Ouchi introduced Co-Cr sputtered thin films as a candidate for perpendicular magnetic recording materials with a high storage density.[1,2] The fiber textured growth of these films leads to a magnetic easy axis perpendicular to the film surface and an appropriate external stray field of the magnetic domains,[3,4] as was demanded for this type of magnetic recording media.

Some years later Fisher and co-workers[5] measured an unexpected high saturation magnetization in Co-Cr sputtered thin films: This led to the idea that the material may be phase separated and furthermore to the hope that such a phase separation could result in a structure of Co-rich ferromagnetic domains within a paramagnetic matrix. In this manner the size of the magnetic domains could be reduced and the magnetic storage capacity in the films could be increased.

To demonstrate the presence of phase separation in Co-Cr thin films, research has been performed. However, investigations by x-ray diffraction or transmission electron microscopy (TEM) were restricted by the fact that the atomic size mismatch and the scattering contrast between Co and Cr is small. After treating the prepared TEM samples with a preferentially Co dissolving etching solution, Maeda and co-workers[6] finally observed a stripe pattern they called Chrysanthemum-like pattern (CP structure). The period of this pattern was about 8 nm. It was found to be dependent on the sputtering conditions, such as the substrate temperature,[7] the Cr concentration, and the film thickness (the CP structure was found to be most pronounced between 15 and 24 at. % Cr at 473 K in 200 nm thin films).[8,9] Maeda and Takahashi mentioned,[9] that because the etching solution preferentially removes the Co from the sputtered films the CP structure should correspond to concentration variations. Investigations by Yoshida and co-workers[10] with nuclear magnetic resonance confirmed this conclusion. Hono *et al.*[11–13] and our group[14,15] investigated Co-Cr sputtered films with atom probe field-ion microscopy and found concentration modulations between about 8 at. % and 40 at. % Cr in the sputtered films.

However, the origin of these concentration modulations has not yet been identified. Hono *et al.* have proposed that the concentration inhomogeneity in the sputtered film is due to a dynamic phase separation during the sputtering process.[16] In such a case surface diffusion during the deposition process may be responsible for the decomposition. Consequently, the modulated structure should only appear in thin films but not in bulk materials: hitherto, such a phase separation has not been detected within bulk alloys.[17] Maeda has proposed an initial diffusion of the components along grain boundaries and subsequently short-range diffusion as film growth proceeded.[18] In an earlier paper, the author suggested a process similar to a spinodal decomposition, to explain the relatively uniform periodicity of the etching lines.[7] In this case, decomposition should also appear in bulk materials in close vicinity to grain boundaries, depending on the bulk diffusivity at low temperatures.

To study the origin of the concentration modulation, we investigated the microstructure and local composition of sputtered Co-20 at. % Cr films, and bulk alloys of the same composition with the field-ion microscope (FIM) including a time-of-flight mass spectrometer [atom probe (AP)]. With the Göttingen AP-FIM the chemical analysis can be done with a nanometer lateral resolution, and on an atomic scale in

depth. In addition to the AP-FIM measurements, we analyzed the samples with TEM after etching using the procedure proposed by Maeda and Takahashi, in order to get information about the morphology on a larger length scale. By comparing of the results obtained with these two methods, concentration modulations and etching structures can be correlated directly.

The origin of the observed modulated structure will be discussed in terms of the thermodynamics and the kinetics of the system. Therefore the experimental results will be compared with a metastable Co-Cr phase diagram that was calculated by the CALPHAD method (CALculation of PHAse Diagrams, details concerning this Co-Cr phase diagram are described in Refs. 19 or 20).[21] Additionally, the diffusivity of the Co-Cr system will be studied in order to obtain information about the dominant diffusion mechanism. The low-temperature diffusivity will be determined by an *in situ* x-ray-diffraction heating experiment of a Co/Cr multilayer.

II. EXPERIMENTAL DETAILS

Co-22 at. % Cr alloy films of 3 μm thickness were sputtered from a Co-22 at. % Cr alloy target at 1 Pa Ar pressure onto a Cu-coated Si substrate at a temperature of 473 K.

Co-20 at. % Cr bulk alloys were prepared by arc melting under 1×10^{-3} Pa Ar pressure from 99.999% Co and 99.99% Cr pellets. Subsequently, some samples were sealed in glass tubes under Ar atmosphere, homogenized at 1023 K for 120 h and then quenched into water by opening the glass tube or slowly cooled down within the glass tube. To realize a higher cooling rate other alloys were splat quenched from the melt. The compositions of the samples were determined by electron microprobe analyses.

The analyses with the FIM/AP require samples in the shape of tips with a radius of curvature between 50 and 200 nm at the apex. Therefore FIM tips from films of 3 μm were prepared by a lithography technique[13] and electropolished afterwards. Tips from bulk material were conventionally produced by grinding and subsequently electropolishing in 3 vol % perchloric acid in acetic acid with 20-12 V dc at room temperature. The AP analyses were carried out at 50 K tip temperature with a background pressure of about 3×10^{-7} Pa. FIM images were taken in a 1×10^{-4} Pa He and 5×10^{-4} Pa Ne gas mixture. The pulse-to-total-voltage fraction was kept constant at 16%.

The TEM studies were performed at room temperature using a Philips EM400. The 3 μm-thick films and the bulk samples were thinned to electron transparency by ion milling (with sample rotation at 30°) from both sides, and subsequent wet etching in 1.25 vol % HNO_3 and 0.18 vol % HCL in H_2O for 2 h to remove the Co. Hence the specimens for the AP-FIM and the TEM analyses both originate from the middle of the bulk and thin-film samples. The part of the sample, where the AP-FIM analyses and the TEM analyses were performed are comparable.

Co/Cr multilayer films with 10 nm pair thickness and a 1:1 thickness ratio were prepared by sputtering from elemental targets (both 99.99%) onto rotating sapphire substrates at room temperature using a computer controlled shutter. The base pressure prior to the deposition was 3×10^{-7} Pa, and the films with total thickness of 2 μm were deposited in a 0.37 Pa argon ambient at typical rates of 0.5 nm/s.

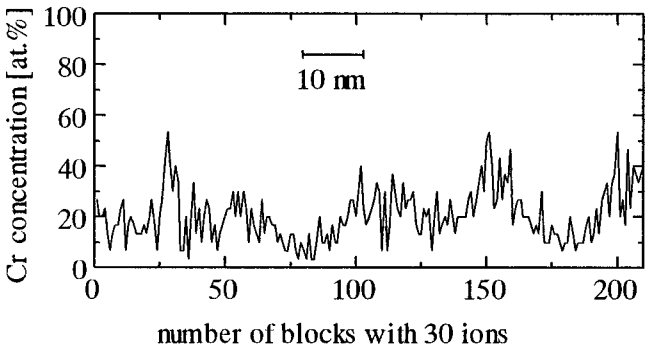

FIG. 1. Concentration depth profile of a Co-22 at. % Cr alloy film which was sputtered at 473 K substrate temperature. The concentration varies between 8 at. % Cr and 40 at. % Cr on a 10 nm scale.

Co-K_α x-ray diffraction was employed using a Siemens D5000 powder diffractometer, equipped with a high-vacuum hot stage and a position-sensitive detector. For measurements that were performed at elevated temperatures, the samples were heated at a rate of 1 K/s to the desired temperatures where isothermal x-ray scans were carried out. The temperature interval between two consecutive measurements was 20 K. Since each scan took 30 min, the average heating rate in these experiments was 0.67 K/min.

III. RESULTS

A. Concentration profiles and microstructure

Figure 1 shows a concentration depth profile of an AP measurement performed using a Co-22 at. % Cr alloy film which was deposited at 473 K substrate temperature. The concentration was determined by averaging over 30 atoms representing one block. The marked depth scale of 10 nm in the AP concentration profiles is understood as a mean scale since the magnification generally decreases during the AP measurement. A depth of about 80 nm of the sample was analyzed. It can be seen that concentration variations on a 10 nm scale are present where a Cr-poor phase with about 8 at. % Cr alternates with a Cr-rich phase which contains about 40 at. % Cr.

A TEM micrograph of a Co selectively etched sample of the same type of sputtered alloy film is shown in Fig. 2. The grain size varies from 20 to several 100 nm. Bright etching lines with a period of about 10 nm can be seen (arrows). In many grains these lines are oriented predominately perpendicular to the grain boundaries. They partly appear in the entire grain (double arrow) and have a maximum length of about 150 nm.

In addition, areas were found where no long-range concentration modulation could be determined with AP. Within these areas 1–2 nm Co-rich clusters could be detected. These clusters also appeared within films that where sputtered at room temperature (for details see Ref. 14 or 15).

In conclusion, concentration modulations on a 10 nm scale are present within the grains. They appear to be identical with the etching lines in the TEM images. The microstructure of these etching lines indicates that the decomposition process may have started at grain boundaries, and has grown in the interior of the grains.

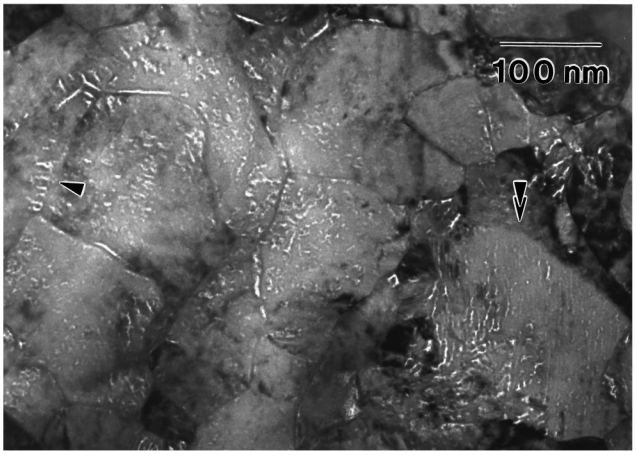

FIG. 2. TEM micrograph of a Co selectively etched Co-22 at. % Cr alloy film which was deposited at 473 K. Bright lines with a period of about 10 nm can be seen (for example, below the arrow). The period length is similar to that of the concentration variations shown in Fig. 1. In some grains lines that run through the whole grain with a length of about 150 nm can be seen (doubled arrow).

In all bulk samples that were cooled down from the homogenization temperature at different cooling rates, concentrations were determined by AP that significantly deviate from the overall concentration. These measurements demonstrate that phase separation also occurs in bulk alloys.

In the slowly cooled sample several concentration steps were measured, as can be seen in the concentration depth profile in Fig. 3(a). The concentration was determined using 50 atoms in each block. It varies between 40 at. % Cr and 8 at. % on a several 10 nm scale. In an analysis depth of about 90 nm (block number 420) a concentration boundary was penetrated perpendicularly. This can be seen by the sharp concentration step, as is shown in detail in Fig. 3(b). The concentration changes from $38(\pm 5)$ at. % Cr to 4.3 (± 1.3) at. % Cr within two atomic layers. In a depth of about 160 nm (block number 790) in Fig. 3(a) a concentration of 20 at. % Cr was measured, indicating that phase separation has not occurred in this region. In a depth of 220 nm (block number 1090) the concentration modulation starts again.

TEM studies of etched bulk samples show stripe structures, as can be seen in Fig. 4. These structures were not found in unetched foils because of the small scattering contrast between Co and Cr. With a typical distance of about 40 nm, bright lines that correspond to previously Co-rich regions can be seen. The measured length scale is in good consistency with the length scale determined from the AP analyses.

These experimental results demonstrate that phase separation has taken place in sputtered films as well as in bulk materials. Since both in thin films and in bulk materials the decomposition microstructure shows a striped line structure, we conclude that the origin of this microstructure is the same. With the aim to study this origin in more detail, thermodynamics and kinetics of the Co-Cr system will be analyzed in the following sections.

B. Thermodynamics of the Co-Cr system

In order to get a phase diagram from the available thermodynamic data that includes recent experimental values,

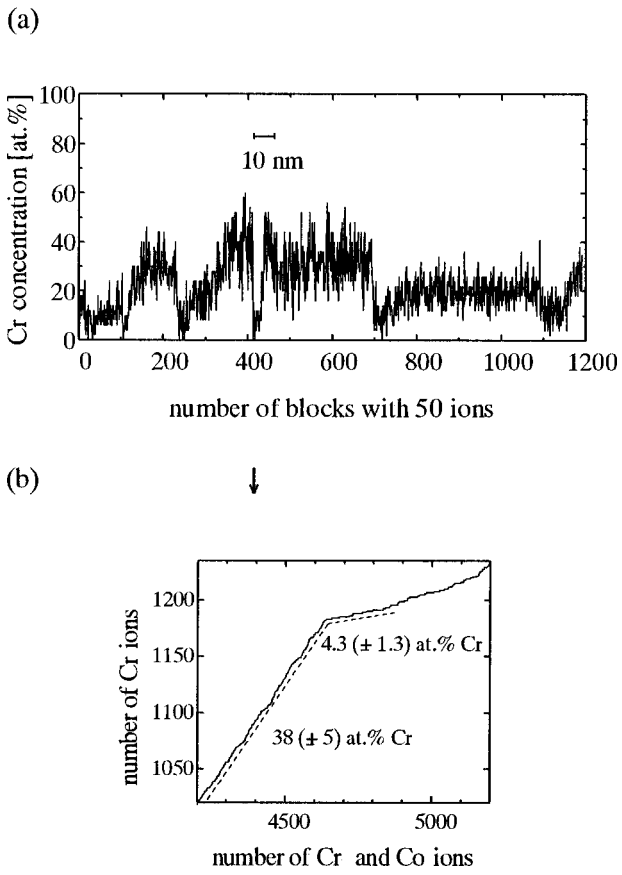

FIG. 3. (a) Concentration depth profile of a slowly cooled Co-20 at. % Cr bulk alloy. The concentrations were determined using 50 atoms in each block. They vary on a larger length scale of about 40 nm. From the concentration step after 90 nm (420 blocks), plotted as a ladder diagram in (b), the maximum concentration can be determined to be 38 at. % Cr, whereas the minimum Cr concentration is about 4.3 at. % Cr.

we have calculated the Gibbs energies of the Co-Cr system by the CALPHAD method.[20,21] In the calculation we have considered the concentration and temperature dependence of the Gibbs energy ΔG for each phase using a regular solution type model

$$\Delta G = c_{\mathrm{Co}} G^0_{\mathrm{Co}} + c_{\mathrm{Cr}} G^0_{\mathrm{Cr}} - TS^{\mathrm{mix}} + \Delta G^{\mathrm{ex}} + \Delta G^{\mathrm{mag}}. \quad (1)$$

c_{Co} and c_{Cr} are the atomic concentrations of Co and Cr, respectively. S^{mix} is the ideal entropy of mixing, and T is the temperature. The phase stability values G^0_{Co} and G^0_{Cr} were taken from the compilation of Dinsdale.[22] Deviations from the ideal solution model are included in the excess free-energy term ΔG^{ex} that we have written, in the Redlich-Kister description,[23] by

$$\Delta G^{\mathrm{ex}} = A_1 c_{\mathrm{Co}} c_{\mathrm{Cr}} + A_2 c_{\mathrm{Co}} c_{\mathrm{Cr}} (c_{\mathrm{Co}} - c_{\mathrm{Cr}}) + B_1 T c_{\mathrm{Co}} c_{\mathrm{Cr}}, \quad (2)$$

where the coefficients A_1, A_2, and B_1 were determined by fits to a large number of experimental data, essentially those summarized in Ref. 24. Magnetic contributions to the Gibbs energies are considered, too: they are included in the phase stability values of Co and in the additional magnetic term ΔG^{mag} following the description of Hillert and Jarl.[25] Experi-

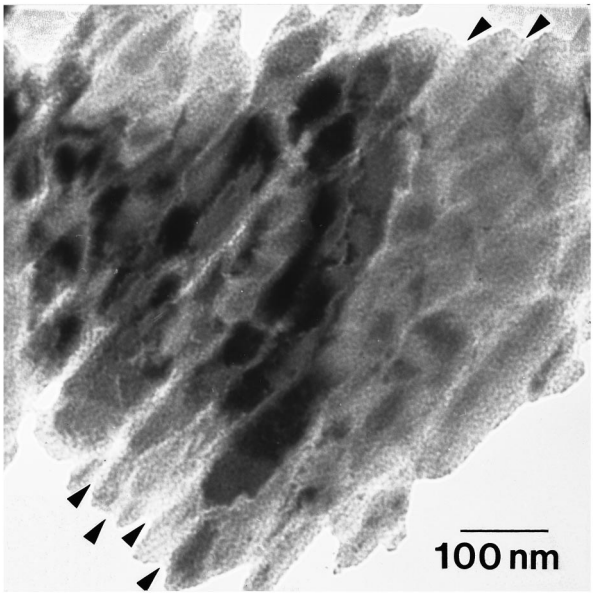

FIG. 4. TEM micrograph taken from a Co selectively etched Co-20 at. % Cr bulk alloy. Bright lines can be seen with a period of about 40 nm. They correspond to previously Co-rich regions. This length scale is consistent to the length scale of the AP analyses shown in Fig. 3(a).

mental magnetic data such as the Curie temperature and the number of Bohr magnetons per atom as a function of composition and temperature are important input data for the calculation. Details of the calculation will be presented in a separate paper.[19]

To compare our experimental results with these Gibbs energies, a metastable phase diagram of the Co-Cr system that excludes the σ phase has been considered. This is because the experiments have shown that the formation of the σ phase is kinetically suppressed even in the bulk alloys. Rather, only the hexagonal-closed-packed (hcp) structure was found in FIM images and TEM diffraction patterns. Such a kinetic suppression of complex intermetallic phases has been found in many other alloys. The σ phase contains 30 atoms in its complex tetragonal elementary cell. The metastable phase diagram is shown in Fig. 5(a) by the full lines. For comparison the stable equilibrium phase diagram that includes the sigma phase (σ) is drawn in dashed lines.

On the Co-rich low-temperature side a magnetically induced miscibility gap between ferromagnetic (f) and paramagnetic (p) hcp phases can be seen (such a gap occurs in the face-centered-cubic (fcc) phase as well). In the metastable equilibrium the magnetically induced miscibility gap between ferromagnetic and paramagnetic hcp phase is a dominant feature at lower temperatures. The experimentally obtained data at about 40 at. % Cr can only be described by the metastable phase diagram, not by the equilibrium phase diagram.

The influence of the magnetic ordering on the Gibbs energy ΔG of the hcp phase can be seen in detail in Fig. 5(b) at a temperature of 473 K. The Co-Cr system is chemically miscible, shown by the dashed line. However, the magnetic ordering stabilizes the hcp phase at low Cr concentrations with respect to a nonmagnetic hcp phase. Since the magnetic

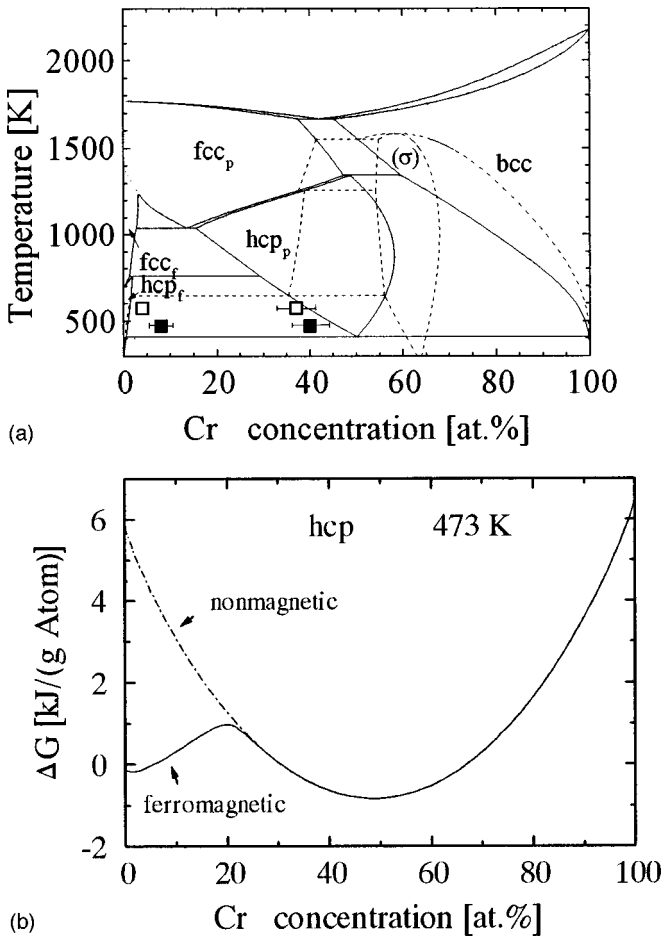

FIG. 5. (a) Metastable phase diagram of the Co-Cr system obtained when the sigma phase (σ) is not taken into account (full lines) and stable equilibrium phase diagram (dashed lines). The experimental data are plotted as squares: ■, obtained from the sputtered film; □, from the bulk alloy. A miscibility gap between Co-rich hcp ferromagnetic phase (hcp_f) and Co-poor hcp paramagnetic phase (hcp_p) can be seen between 410 and 760 K. (b) Gibbs energy ΔG of the hcp phase at 473 K. The Co-Cr system is chemically miscible, shown by the dashed line. The magnetic ordering lowers the Gibbs energy at low Cr concentrations and thus induces a miscibility gap. The Gibbs energy reference states are ferromagnetic hcp Co and bcc Cr.

moment of the magnetically ordered hcp phase and its Curie temperature increases with the Co content,[26,27] the decrease of ΔG increases with the Co content thus inducing a miscibility gap.

The Cr-rich side of the miscibility gap is located at much higher Cr concentrations than expected in former phase diagrams.[28] This is due to an inclusion of recent experimental data in our calculations, in which particularly the magnetic description deviates from previous works. The concentration dependence of the Curie temperature mainly determines the width of the miscibility gap which, in our calculation, is wider than that determined by Hasebe and co-workers and extrapolates to lower temperatures.[28] We note that our calculations were performed independently from our experimental results, thus the width of the miscibility gap is not determined by our experimental data.

With an overall concentration of 20 at. % Cr our samples

are located within this magnetically induced miscibility gap. The formation of two hcp phases is therefore expected to occur between 410 and 760 K, assuming that the kinetics are sufficient for the development of the metastable equilibrium. The experimentally obtained concentrations fit quite well to this calculated metastable miscibility gap, as can be seen from the metastable phase diagram in Fig. 5(a). Hence, the Cr-poor phase exhibits ferromagnetic ordering, whereas the Cr-rich phase is a paramagnetic one.

C. Diffusivities in the Co-Cr system

The above results have shown that a metastable equilibrium between ferromagnetic and paramagnetic hcp phases has developed in all samples investigated. From this fact we conclude that the kinetics of decomposition are very fast. To focus on diffusivities in the system, experimental bulk interdiffusion coefficients for Co in Co-21.8 at. % Cr and Co-26.9 at. % Cr alloys, obtained for temperatures above 1273 K by Green *et al.*,[29] are plotted (in open circles) in Fig. 6. Since the extrapolation of these data to 473 K goes over several decades in the diffusivity, we additionally determined the interdiffusion coefficient at lower temperatures by a multilayer experiment. A sputtered Co/Cr multilayer with a pair thickness of $\lambda = 10$ nm was annealed at temperatures ranging from 573 to 1133 K, in steps of 20 K every 30 min. At each temperature an *in situ* x-ray-diffraction pattern was recorded. Typical patterns are shown in Fig. 7. The uppermost pattern is obtained from the as-sputtered multilayer, and shows a typical pattern as it was also observed by Boher[30] and Sato[31] on comparable Co/Cr multilayers. The pattern exhibits a number of satellites about the Bragg peaks of Co and Cr, as is typical of multilayer films when the interfaces between the constituents are coherent. At temperatures above 833 K diffusion sets in, as can be seen from the intensity change of the x-ray peaks. The pattern changes from that of the as-sputtered multilayer to that of an hcp phase at 873 K. Starting at 893 K additional σ phase reflections appear, indicating the formation of the equilibrium phases hcp plus σ. Small peak shifts can be determined that might originate from internal stresses of the multilayered film.

Assuming a diffusion-controlled growth of the new phases, the interdiffusion coefficient can be estimated by inserting the maximum thickness of the product phase (5 nm at each interface) as diffusion distance x, and the diffusion time of 30 min into a parabolic growth law:

$$D_V = \frac{x^2}{2t} = 6.9 \times 10^{-21} \frac{m^2}{s} \quad \text{at } 873 \text{ K}, \tag{3}$$

for Co 50 at. % Cr. The thermodynamic factors of a 22 at. % Cr alloy and the 50 at. % Cr alloy can be determined from the Gibbs energies at 873 K to be 1.7 and 2.4, respectively. Taking this into account yields a diffusion coefficient $D_V = 4.9 \times 10^{-21}$ m^2/s at 873 K for the Co-22 at. % Cr alloy, plotted in bold circle in Fig. 6. It is in good agreement with the low-temperature extrapolation of the diffusion coefficients determined by Green *et al.*, as can be seen from the straight line in Fig. 6. Taking this value into consideration an activation energy of 2.8 eV and a preexponential factor of 5.3×10^{-5} m^2/s were obtained. Green *et al.* determined from their high-temperature data an activation energy of 2.62 eV and a preexponential factor of 1.26×10^{-5} m^2/s.

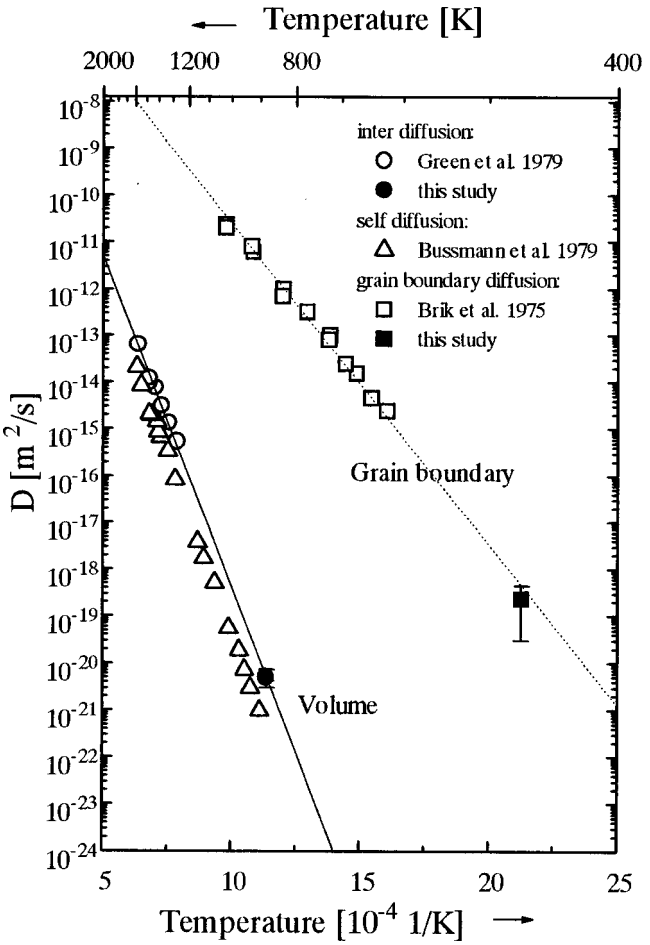

FIG. 6. Volume and grain-boundary diffusion coefficients of the Co-Cr system: ○, Co inter diffusion coefficients in a Co-21.8 at. % Cr alloy after Green *et al.* (Ref. 29); △, coefficients of self diffusion of Co after Bussmann *et al.* (Ref. 32); and ●, the value obtained in the present investigation using multilayer films are plotted vs the temperature. An extrapolation to the relevant temperatures of about 500 K leads to a volume diffusion coefficient of less than 10^{-30} m^2/s. □, the grain-boundary self-diffusion coefficients of Co after Brik and co-workers (Ref. 33) are plotted under assumption of a boundary width of 1 nm. An extrapolation to 500 K shows that the grain-boundary diffusion coefficient is still in the order of 10^{-18} m^2/s. This agrees with the value experimentally obtained under the assumption of discontinuous precipitation process in the alloy film, ■.

Self-diffusion coefficients of Co obtained by Bussmann *et al.*[32] are also plotted in Fig. 6, indicating a comparable temperature dependence.

Hence, the volume diffusion coefficient D_V of Co-22 at. % Cr alloys is very small at low temperatures: The extrapolation to 500 K results in a volume diffusion coefficient of less than 10^{-30} m^2/s. This means that volume diffusion can be neglected at low temperatures. Therefore grain-boundary diffusion or surface diffusion have to be taken into consideration as active diffusion mechanisms at lower temperatures.

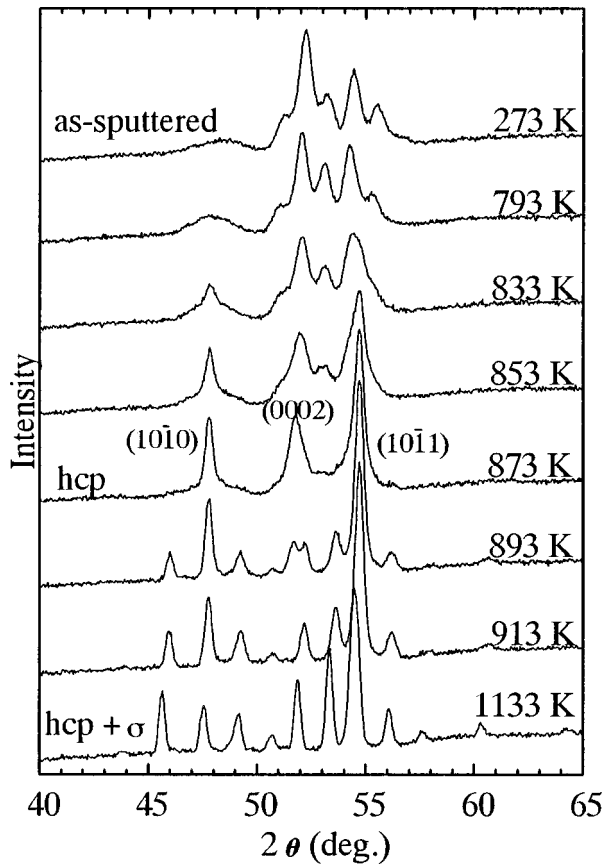

FIG. 7. X-ray patterns of a Co/Cr multilayer with 10 nm pair thickness and 1:1 thickness ratio during annealing. Above 833 K changes in the pattern can be observed indicating the onset of diffusion. At 873 K a hcp structure has developed and above 893 K the patterns of the equilibrium phases σ and hcp are visible.

IV. DISCUSSION

The metastable phase diagram in Fig. 4 demonstrates that at temperatures below 800 K the overall concentration of the analyzed alloys is located within a miscibility gap between ferromagnetic and paramagnetic phases. Therefore, a driving force for phase separation exists that leads to the formation of a metastable thermodynamic equilibrium between two hcp phases. At temperatures of about 500 K concentrations of about 1 at. % Cr and 42 at. % Cr are expected to be in metastable equilibrium.

Since the bulk diffusivity is very small at these temperatures, bulk diffusion cannot explain the formation of long-range concentration modulations. In other words, bulk diffusion can be excluded as the rate controlling mechanism for the observed decomposition. Because of the negligible bulk diffusion, it can also be ruled out that spinodal decomposition is responsible for the decomposition. Rather, other diffusion processes such as surface diffusion or grain-boundary diffusion must be responsible for the measured compositional modulations. Since the concentration modulation also appears in bulk alloys, decomposition by surface diffusion during the sample preparation cannot be responsible for its formation.

Hence grain-boundary diffusion, known to be much faster than bulk diffusion at low temperatures, has to be taken into account. Grain-boundary interdiffusivities for Cr or Co in the

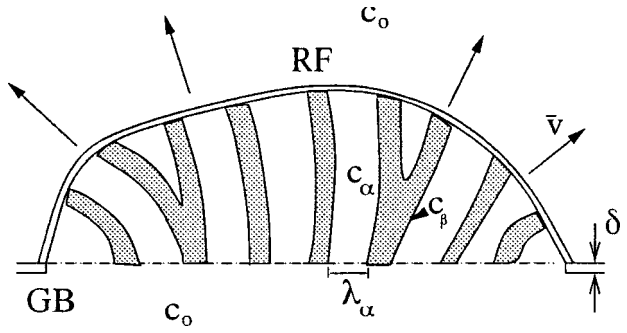

FIG. 8. Schematic illustration of a discontinuous precipitation reaction cell. The reaction starts at the grain boundary. By grain-boundary diffusion the reaction front propagates with a mean velocity $\bar{v}$ into the supersaturated matrix, leaving a lamellae structure with a lamellae width λ_α behind. The concentrations c_α and c_β are those of the decomposed phases.

alloy are not published yet. Grain-boundary self-diffusivities (between 1023 and 623 K) of pure Co were obtained by Brik and co-workers.[33] By assuming a grain-boundary width of 1 nm, self-diffusion coefficients can be determined that are plotted with open squares in Fig. 6. The extrapolation to low temperatures leads to a Co self-diffusion coefficient of about 10^{-18} m^2/s at 473 K. This diffusion coefficient appears large enough to account for the occurrence of phase separation at low temperatures.

A phase separation mechanism including grain-boundary diffusion and resulting in a lamellae structure of the decomposed alloys is the discontinuous precipitation mechanism.[34] A discontinuous reaction cell is schematically shown in Fig. 8. The reaction front (RF) is propagating with a mean velocity $\bar{v}$ into the supersaturated matrix with a concentration c_0 after heterogeneous nucleation at a grain boundary (GB). Diffusion along this reaction front, comparable to diffusion along a grain boundary, leads to the phase separation. A lamellae structure of separated phases with concentrations c_α and c_β is left behind the propagating reaction front.

Using the theory of Cahn,[34] Bögel and Gust[35] have given a general equation for the discontinuous precipitation, in which the reaction front diffusivity, δD_{RF}, is given by

$$\delta D_{\mathrm{RF}} = \frac{1}{a_c}\,\frac{RT}{-\Delta G}\,\bar{v}\,\overline{\lambda}_\alpha^2, \tag{4}$$

where λ_α is the lamellae spacing of the α lamellae, T is the annealing temperature, ΔG is the driving force, δ is the thickness of the reaction front, and R is the general gas constant. The quantity a_c introduced by Cahn is given by the equation

$$\frac{c_0-\overline{c_\alpha}}{c_0-c_\alpha^e} = \left[\tanh\left(\sqrt{\frac{a_c}{4}}\right)\right] : \sqrt{\frac{a_c}{4}} \tag{5}$$

and includes a dependence from the concentration of the supersaturated matrix with $c_0 = 22$ at. % Cr, the equilibrium concentration of the α phase with $c_\alpha^e = 0.5$ at. % Cr obtained from the phase diagram, and its experimentally obtained mean concentration $\overline{c_\alpha} = 8$ at. % Cr. The difference between the experimentally obtained mean concentration $\overline{c_\alpha}$ and the equilibrium concentration c_α^e reveals the nonequilibrium

conditions of the discontinuous precipitation process. For $\overline{c_\alpha}=c_\alpha^e$ that means $a_c=0$, the reaction front diffusivity is infinite. Thus, the occurrence of a difference between $\overline{c_\alpha}$ and c_α^e makes it possible to determine a limited reaction front diffusivity. This requires a material with very slow bulk diffusivity. As mentioned above, the analyzed Co-Cr alloy possesses slow bulk diffusivity at low temperatures. Graphical solution leads to $a_c=7.18$. The reaction front diffusivity in general can be set equal to the grain-boundary diffusivity.

This equation makes it possible to determine the grain-boundary diffusivity if the mean reaction front velocity can be estimated. The experimental results have shown that at a substrate temperature of 473 K lamellae with a length l of about 150 nm (see Fig. 2) can be formed during a sputtering time of $t=2$ h. From this a reaction front velocity of $\overline{v}=1/t=2.1\times10^{-2}$ nm/s can be obtained. With Eqs. (4) and (5) a grain-boundary diffusivity can be determined to

$$\delta D_{\mathrm{GB}}=2.3\times10^{-28}\,\frac{m^3}{s}. \tag{6}$$

Assuming a $\delta=1$ nm, a diffusion coefficient of $D_{\mathrm{GB}}=2.3\times10^{-19}$ m^2/s is obtained and plotted in bold square in Fig. 6. The value is in good agreement with the low-temperature extrapolation of the grain-boundary diffusivity data of Brik,[33] as can be seen from the dashed line in Fig. 6.

This result strongly supports the assumption, that discontinuous precipitation is the phase-separation mechanism at the experimentally studied temperatures and concentrations. It also demonstrates that during the sputtering procedure, where the film is kept at an elevated temperature, the observed composition modulation can develop in the already deposited part of the film. Hence the *time* of the sputtering (and simultaneously annealing) procedure can be an important structure determining parameter: The shorter the film is kept at elevated temperatures, the smaller is the decomposed volume in the Co-Cr alloy film. The result also indicates that the composition modulations should be dependent on the sputtering conditions.

Describing the decomposition of bulk alloys using the discontinuous precipitation approach at a temperature of 573 K (taken as a mean temperature during the cooling procedure of the slow-cooled bulk sample) leads to reaction front velocities of about 0.2 nm/s. Here the grain-boundary diffusivity $D=1.9\times10^{-16}$ m^2/s was taken at 573 K from the fit to the data of Brik[33] and the value deduced above, as indicated by the dashed line in Fig. 6. The factor $a_c=2.4$ was determined by using an equilibrium concentration of 1.2 at. % Cr obtained from the metastable phase diagram shown in Fig. 5(a), the experimentally determined minimum concentration of 4.3 at. % Cr and the mean concentration of 20 at. % Cr. The gain of Gibbs energy $\Delta G=1$ kJ/mol was derived from the Gibbs Energy function at 573 K. A lamellae width of 20 nm was used that results from half of the typical lamellae distance obtained from Fig. 4. Such a reaction front propagates by about 150 nm in 10 min. from the grain boundaries into the grains. Assuming a reaction temperature of 673 K and using the corresponding data, the reaction front propagates by about 1.3 μm within 1 min. Additionally, during the cooling process frozen-in vacancies might increase the velocity of the reaction front. This indicates that discontinuous precipitation can lead to a noticeable amount of phase separated volume also in Co-20 at. % Cr bulk materials having grain sizes of several μm, during the cooling process.

In thin films with small grains, discontinuous reaction cells nucleating at all grain boundaries should result in a lamellae structure leading to the CP structure observed after the etching procedure. The dependence of this lamellae structure on substrate temperature, on Cr concentration, and on the thickness of the sample, might be correlated with the dependence of the discontinuous precipitation reaction on reaction temperature, the gain of Gibbs energy, the annealing time, and the grain size.

In conclusion, discontinuous precipitation is a decomposition mechanism that can explain all observed features within Co-20 at. % Cr bulk and thin-film alloys.

V. SUMMARY

The decomposition in Co-20 at. % Cr sputtered films and bulk alloys was analyzed using transmission electron microscopy and field-ion microscopy with atom probe. It was shown that thin-film and bulk alloys are decomposed into regions of about 8 at. % Cr and 40 at. % Cr, respectively. The observed concentrations are in good agreement with the solubilities that results from a magnetically induced metastable miscibility gap at the Co-rich low-temperature side of the Co-Cr system. It is shown that bulk diffusion can be neglected as rate controlling process. Also, surface diffusion can be disregarded since decomposition also occurs in bulk alloys. Taking into account the morphology of the concentration modulations and the result that the decomposition occurs via grain-boundary diffusion, it is concluded that discontinuous precipitation is the process that controls the decomposition. Using the theory of discontinuous precipitation of Bögel and Gust, a reaction front diffusivity can be determined that fits to the extrapolation of higher temperature grain-boundary diffusivities. Furthermore, the lamellae structures in bulk alloys and the CP structure occurring in etched thin films can be explained with this decomposition mechanism. In summary, the discontinuous precipitation process is the decomposition mechanism that can explain the formation of the observed composition modulations in Co-20 at. % Cr thin-film and bulk alloys.

ACKNOWLEDGMENTS

The authors would like to acknowledge the support of their advisor P. Haasen. They also wish to thank D. Isheim, R. Kirchheim, and R. Wagner for helpful discussions. K. Hono (National Research Institute for Metals, Tsukuba) is thanked for kindly providing the lithography samples. They are grateful to H. L. Lukas (Max-Planck-Institut für Metallforschung, Stuttgart) who provided the CALPHAD software. This work was supported by the Deutsche Forschungsgemeinschaft via Sonderforschungsbereich 345.

[1] S. Iwasaki and K. Ouchi, IEEE Trans. Magn. **14**, 849 (1978).
[2] J. H. Judy, MRS Bull. **15**, 63 (1990).
[3] E. Kneller, *Ferromagnetismus* (Springer, Berlin, 1962).
[4] W. Andrä, H. Danan, and R. Mattheis, Phys. Status Solidi A **125**, 9 (1991).
[5] R. D. Fisher, V. S. Au-Yeung, and B. B. Sabo, IEEE Trans. Magn. **20**, 806 (1984).
[6] Y. Maeda, S. Hirono, and M. Asahi, Jpn. J. Appl. Phys. **24**, L951 (1985).
[7] Y. Maeda and M. Asahi, IEEE Trans. Magn. **23**, 2061 (1987).
[8] Y. Maeda, M. Asahi, and M. Seki, Jpn. J. Appl. Phys. **25**, L668 (1986).
[9] Y. Maeda and M. Takahashi, IEEE Trans. Magn. **24**, 3012 (1988).
[10] K. Yoshida, H. Kakibayashi, and H. Yasuoka, J. Appl. Phys. **68**, 705 (1990).
[11] K. Hono, S. S. Babu, Y. Maeda, N. Hasegawa, and T. Sakurai, Appl. Phys. Lett. **62**, 2504 (1993).
[12] K. Hono, Y. Maeda, J.-L. Li, and T. Sakurai, IEEE Trans. Magn. **29**, 3745 (1993).
[13] N. Hasegawa, K. Hono, R. Okano, H. Fujimori, and T. Sakurai, Appl. Surf. Sci. **67**, 407 (1993).
[14] A. Pundt, R. Busch, and C. Michaelsen, in *Polycrystalline Thin Films—Structure, Texture, Properties and Applications*, edited by K. Barmak *et al.*, MRS Symposia Proceedings No. 343 (Materials Research Society, Pittsburgh, 1994), p. 309.
[15] A. Pundt and C. Michaelsen, Appl. Surf. Sci. **87/88**, 264 (1995).
[16] K. Hono, Y. Maeda, J.-L. Li, and T. Sakurai, J. Magn. Magn. Mater. **110**, L254 (1992).
[17] L. H. Chan, G. Thomas, and J.-S. Gau, J. Magn. Magn. Mater. **79**, 95 (1989).
[18] Y. Maeda, Adv. Mater. **5**, 210 (1993).
[19] A. Pundt, C. Michaelsen, F. Gärtner, and R. Bormann (unpublished).
[20] A. Pundt, Ph.D. thesis, Georg-August-Universität, Göttingen, 1995.
[21] H. L. Lukas, J. Weiss, and E.-T. Henig, CALPHAD: Comput. Coupling Phase Diagrams Thermochem. **6**, 229 (1982).
[22] A. T. Dinsdale, NPL Report DMA(A) No. 195, 1989 (unpublished).
[23] O. Redlich and A. T. Kister, Ind. Eng. Chem. **40**, 345 (1948).
[24] K. Ishida and T. Nishizawa, Bull. Alloy Phase Diagrams **11**, 357 (1990).
[25] M. Hillert and M. Jarl, CALPHAD: Comput. Coupling Phase Diagrams Thermochem. **2**, 227 (1978).
[26] T. Farcas, Ann. Phys. (Leipzig) **8**, 146 (1937).
[27] F. Bolzoni, F. Leccabue, R. Panizzieri, and L. Pareti, J. Magn. Magn. Mater. **31-34**, 845 (1983).
[28] M. Hasebe, K. Oikawa, and T. Nishizawa, J. Jpn. Inst. Met. **46**, 577 (1982).
[29] A. Green, D. P. Whittle, J. Stringer, and N. Swindells, Scr. Metall. **7**, 1079 (1973).
[30] P. Boher, J. Appl. Phys. **70**, 5507 (1991).
[31] N. Sato, J. Appl. Phys. **61**, 1979 (1987).
[32] W. Bussmann, C. Herzig, W. Remp, K. Maier, and H. Mehrer, Phys. Status Solidi A **56**, 87 (1979).
[33] V. B. Brik, L. N. Larikov, and V. M. Fal'chenko, Ukr. Fiz. Zh. **20**, 397 (1975).
[34] J. W. Cahn, Acta Metall. **7**, 18 (1959).
[35] A. Bögel and W. Gust, Z. Metallkd. **79**, 296 (1988).